the range of values of $\Delta H^{\ddagger}$ and $\Delta S^{\ddagger}$ being well outside the experimental uncertainties in these parameters. A plot of $\Delta H^{\ddagger}$ vs. $\Delta S^{\ddagger}$ (Figure 2) reveals a reasonable isokinetic relationship,[27] with an isokinetic temperature of about 330 K. Although caution should be exercised,[28] the isokinetic correlation supports the existence of a constant mechanism throughout the series.

Macrocycle Structure and the Dissociation Rate. The rates for the nickel complexes of the unsubstituted macrocycles **1**, **3**, **6**, and **7** indicate that there is a clear dependence of the dissociation rate on macrocyclic ring size: the rate constants show a progressive decrease as the macrocyclic ring size increases from 14 to 16 membered followed by a sharp increase for the complex of the 17-membered ring. The occurrence of a minimum rate for the series at the 16-membered ring complex demonstrates dramatically the effect that macrocyclic ring size can have on kinetic lability. In addition, this sequence of kinetic stabilities follows a pattern similar to that of the thermodynamic stabilities (obtained in 95% methanol) which peak at the 16-membered macrocyclic complex.[8,29]

Previous studies involving copper complexes of S_4-donor macrocycles have also demonstrated that ring size strongly influences the dissociation rates but has a smaller effect on the rates of formation.[13] Further, limited kinetic data for two high-spin nickel(II) complexes of N_4-donor macrocycles[18] suggest that the complex of the macrocycle of best fit yields the slowest dissociation rate.

For the present series, hole size considerations suggest that the 16-ring macrocycle provides the best fit for nickel(II). A survey[8] of published data for octahedral nickel(II) indicates a mean (eight distances) nickel–ether oxygen bond distance of 2.15 Å, whereas a mean nickel–nitrogen distance of about 2.10 Å is typical of sp^3-hybridized nitrogens in high-spin macrocyclic nickel complexes.[3] Hence an optimum hole size of 4.25 Å appears reasonable for the present series. This is slightly larger than that of 4.20 Å found (sum of the mean Ni–O and Ni–N distances)[3] for the nickel chloride complex of the 15-membered macrocycle (**3**) but close to that of 4.28 Å found[8] for the nickel complex of the 16-membered analogue (**6**).[30]

Apart from ring size, macrocycle substituents also affect the dissociation rates (Table III). Compared with the case of the corresponding unsubstituted analogues, there is a decrease in the rate of dissociation for the complexes of the N-methylated (**5**) or C-methylated (**2**) derivatives. This diminution of the rate perhaps arises from the methyl groups offering a steric barrier[31] to the folding of the macrocycle which is a necessary step if ligand dissociation is to occur. Other studies[11,32] involving N_4-donor macrocycles have also shown that N-methylation can markedly affect rates of dissociation.

Preliminary studies indicate very different dissociation rates for complexes having a given macrocycle of the present type but incorporating transition-metal ions other than nickel. Such kinetic discrimination shows promise for development of efficient separation techniques for metal ions of the transition series. Further studies in this area are proceeding.

Acknowledgment. L.F.L. and R.J.S. acknowledge the Australian Institute for Nuclear Science and Engineering for a travel grant and the Australian Research Grants Committee for support. We thank Dr. J. T. Baker of the Roche Research Institute of Marine Pharmacology, Sydney, for assistance.

Registry No. **2** dihydrochloride, 72228-66-1; **3** dihydrochloride, 72228-67-2; $NiLCl_2$ (L = **1**), 66793-50-8; $NiLCl_2$ (L = **2**), 72228-93-4; $NiLCl_2$ (L = **3**), 66810-83-1; $NiLCl_2$ (L = **4**), 66793-39-3; $NiLCl_2$ (L = **5**), 66793-41-7; $NiLCl_2$ (L = **6**), 66793-45-1; $NiLCl_2$ (L = **7**), 71375-56-9.

Supplementary Material Available: A complete tabulation of all dissociation rate data (5 pages). Ordering information is given on any current masthead page.

(27) J. E. Leffler and E. Grunwald, "Rates and Equilibria of Organic Reactions", Wiley, New York, 1962, Chapter 9; J. D. Miller and R. J. Prince, *J. Chem. Soc. A*, 1048 (1966); D. Thusius, *Inorg. Chem.*, **10**, 1106 (1971); R. G. Wilkins, "The Study of Kinetics and Mechanism of Reactions of Transition Metal Complexes", Allyn and Bacon, London, 1974; D. M. W. Buck and P. Moore, *J. Chem. Soc., Dalton Trans.*, 2082 (1974); M. U. Fayyaz and M. W. Grant, *Aust. J. Chem.*, **31**, 1439 (1978).

(28) H. P. Bennetto and E. F. Caldin, *J. Chem. Soc., Chem. Commun.*, 599 (1969); *J. Chem. Soc. A*, 2191, 2198 (1971); P. K. Chattopadhyay and J. F. Coetzee, *Inorg. Chem.*, **12**, 113 (1973).

(29) Low solubilities prevented potentiometric measurement of stability constants for the series in water.

(30) An alternative approach for estimating hole size based on the mean distance of the donor atoms from their centroid gives 4.18 Å for the complex of **3** and 4.27 Å for the complex of **6** (see ref 8).

(31) T. S. Turan, *Inorg. Chem.*, **13**, 1584 (1974).

(32) E. K. Barefield and F. Wagner, *Inorg. Chem.*, **12**, 2435 (1973).

Contribution from the Departments of Chemistry, University of Denver, Denver, Colorado 80208, and University of Colorado at Denver, Denver, Colorado 80202

Metal–Nitroxyl Interactions. 14. Bis(hexafluoroacetylacetonato)copper(II) Adducts of Spin-Labeled Pyridines

P. M. BOYMEL, G. R. EATON,* and S. S. EATON

Received October 16, 1979

Spin-labeled ligands have been prepared by condensing pyridine-4-carboxaldehyde, pyridine-3-carboxaldehyde, and pyridine-2-carboxaldehyde with 4-amino-2,2,6,6-tetramethylpiperidinyl-1-oxy. The equilibrium constants have been obtained for the coordination of these ligands to bis(hexafluoroacetylacetonato)copper(II) in CCl_4. The EPR spectra of the 1:1 complexes exhibit electron–electron coupling constants in CCl_4 at room temperature of 43.5, 94.0, and >1000 G for the 4-, 3- (two isomers of complex), and 2-substituted pyridines, respectively. Coupling constants of 71 and 150 G were observed at ca. −190 °C for the 4- and 3-substituted pyridine adducts in toluene glass.

Introduction

The widespread use of spin labels in the study of biological systems has led to considerable interest in the perturbations of the EPR spectra which may occur when a metal ion is also present.[1] We have reported several examples of copper–nitroxyl complexes in which resolved electron–electron coupling is observed in the room-temperature EPR spectra.[2-7] Values

* To whom correspondence should be addressed at the University of Denver.

(1) Eaton, G. R.; Eaton, S. S. *Coord. Chem. Rev.* **1978**, *26*, 207–62.

0020-1669/80/1319-0727$01.00/0

of the coupling constant, J, ranging from 4.8[4] to 2650 G[6] have been found, but the dependence of J on the distance between the copper and the nitroxyl has not been established. We have now prepared the homologous series of spin-labeled pyridines (I–III) and the closely related diamagnetic piperidine derivatives (IV–VI) and examined the equilibria of adduct formation with $Cu(hfac)_2$.[8] The 1:1 adducts of ligands I–VI with

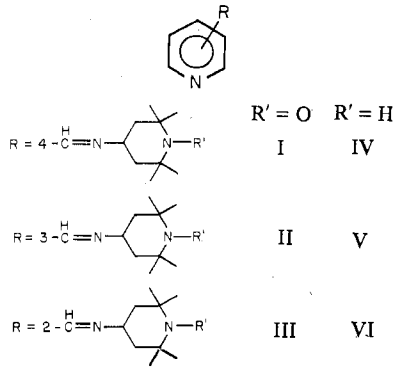

$Cu(hfac)_2$ are denoted VII–XII, respectively. $Cu(hfac)_2$ was chosen because of its high Lewis acidity toward pyridine donors.[9] The complexes with diamagnetic ligands were prepared to aid in the interpretation of the EPR spectra of the copper complexes with paramagnetic ligands.

Experimental Section

Physical Measurements. Infrared spectra were obtained in halocarbon and Nujol mulls on a Perkin-Elmer 337 grating spectrometer. Magnetic susceptibilities were measured on a Bruker Faraday balance with 1 μg sensitivity by using $HgCo(SCN)_4$ as calibrant.[10] Values of μ_{eff} in Bohr magnetons (μ_B) are reported below with the temperature at which the measurement was made and the diamagnetic correction (χ^{dia})[11] used in the calculation given in parentheses. Magnetic susceptibilities are in cgs emu units throughout the following discussion. A value of 60×10^{-6} was assumed for the temperature-independent paramagnetism of copper.[4] Electronic spectra were recorded on a Beckman Acta V spectrometer with the cell compartment thermostated at 20 °C. $Cu(hfac)_2$ and the ligands were sublimed under vacuum before use for spectral studies. CCl_4 and toluene were dried over CaH_2 and distilled under nitrogen. Solutions were prepared in a Kewaunee glovebox. For minimum dissociation and interference from remaining traces of water, concentrations of 5.0×10^{-3}–1.0×10^{-2} M were used for the visible spectra and the EPR spectra. EPR spectra in CCl_4 and toluene solutions were obtained on a Varian E-9 spectrometer as previously described.[4] g values were measured relative to DPPH. All integrated intensities were independent of time. The integrated intensity of the EPR spectra for $Cu(hfac)_2$ in the presence of ligands IV–VI was independent of ligand concentration. All coupling constants are given in gauss except in Table III where values are also given in cm^{-1}. NMR spectra were recorded on a Varian EM-360.

Preparation of Compounds. All starting materials were commercially available and were used as received unless specified otherwise. $Cu(hfac)_2$ was prepared by the literature method.[12]

The following procedure is typical of the method used to prepare the ligands. Purification and characterization data are given below for the remaining ligands.

4-[(2,2,6,6-Tetramethyl-4-piperidyl-1-oxy)iminomethyl]pyridine (I). To a solution of 4-amino-2,2,6,6-tetramethylpiperidinyl-1-oxy (0.500 g, 2.92×10^{-3} mol) in 20 mL of ethanol was added pyridine-4-carboxaldehyde (0.312 g, 2.92×10^{-3} mol). After the solution was refluxed for 2 h, half of the solvent was removed by distillation at atmospheric pressure. The orange precipitate which formed when the mixture was cooled to −20 °C was collected by filtration, washed with ice-cold ether, and sublimed under vacuum at 100 °C: yield 0.715 g (94%); mp 113–114 °C; IR $\nu_{C=N}$ 1645 cm^{-1}; EPR (CCl_4) $g = 2.0062$, $A_N = 15.1$ G; $\mu_{eff} = 1.71$ μ_B (24.5 °C, $\chi^{dia} = -151.6 \times 10^{-6}$). Anal. Calcd for $C_{15}H_{22}N_3O$: C, 69.20; H, 8.52; N, 16.14. Found: C, 69.35; H, 8.22; N, 16.12.

3-[(2,2,6,6-Tetramethyl-4-piperidyl-1-oxy)iminomethyl]pyridine (II): sublimed under vacuum at 90 °C; yield 96%; mp 111–112 °C; IR $\nu_{C=N}$ 1645 cm^{-1}; EPR (CCl_4) $g = 2.0062$, $A_N = 15.2$ G; $\mu_{eff} = 1.63$ μ_B (25 °C, $\chi^{dia} = -151.6 \times 10^{-6}$). Anal. Calcd for $C_{15}H_{22}N_3O$: C, 69.20; H, 8.52; N, 16.14. Found: C, 69.10; H, 8.44; N, 16.06.

2-[(2,2,6,6-Tetramethyl-4-piperidyl-1-oxy)iminomethyl]pyridine (III): sublimed under vacuum at 80 °C; yield 94%; mp 96.5–97.5 °C; IR $\nu_{C=N}$ 1645 cm^{-1}; EPR (CCl_4) $g = 2.0062$, $A_N = 15.2$ G; $\mu_{eff} = 1.66$ μ_B (27 °C, $\chi^{dia} = -151.6 \times 10^{-6}$). Anal. Calcd for $C_{15}H_{22}N_3O$: C, 69.20; H, 8.52; N, 16.14. Found: C, 69.02; H, 8.46; N, 16.16.

4-[(2,2,6,6-Tetramethyl-4-piperidyl)iminomethyl]pyridine (IV): sublimed under vacuum at 110 °C; yield 95%; mp 119.5–120 °C; IR ν_{NH} 3265, $\nu_{C=N}$ 1645 cm^{-1}; NMR (CCl_4) 8.55 (d, $J = 6$ Hz, pyridine α-H), 8.23 (s, azomethine H), 7.45 (d, $J = 6$ Hz, pyridine β-H), 3.63 (m, piperidine 4-H), 1.45 (m, piperidine 3,5-H), 1.12, 1.22 (s, piperidine 2,6-CH_3). Anal. Calcd for $C_{15}H_{23}N_3$: C, 73.43; H, 9.45; N, 17.13. Found: C, 73.26; H, 9.36; N, 16.95.

3-[(2,2,6,6-Tetramethyl-4-piperidyl)iminomethyl]pyridine (V): sublimed under vacuum at 65 °C; yield 92%; mp 77–78 °C; IR ν_{NH} 3265, $\nu_{C=N}$ 1640^{-1} cm^{-1}; NMR (CCl_4) 8.60 (m, pyridine α-H), 8.27 (s, azomethine H), 8.02 (m, pyridine γ-H), 7.20 (m, pyridine β-H), 3.65 (m, piperidine 4-H), 1.50 (m, piperidine 3,5-H), 1.22, 1.12 (s, piperidine 2,6-CH_3). Anal. Calcd for $C_{15}H_{23}N_3$: C, 73.43; H, 9.45; N, 17.13. Found: C, 73.46; H, 9.32; N, 17.20.

2-[(2,2,6,6-Tetramethyl-4-piperidyl)iminomethyl]pyridine (VI): sublimed under vacuum at 55 °C; yield 70%; mp 61–62 °C; IR ν_{NH} 3265, $\nu_{C=N}$ 1645 cm^{-1}; NMR (CCl_4) 8.55 (d, $J = 5$ Hz, pyridine α-H), 8.35 (s, azomethine H), 8.00 (d, $J = 6$ Hz, pyridine γ-H), 7.62, 7.20 (m, pyridine β-H), 3.75 (m, piperidine 4-H), 1.57 (m, piperidine 3,5-H), 1.25, 1.15 (s, piperidine 2,6-CH_3). Anal. Calcd for $C_{15}H_{23}N_3$: C, 73.43; H, 9.45; N, 17.13. Found: C, 73.42; H, 9.32; N, 17.14.

The following procedure is typical of the method used to prepare the $Cu(hfac)_2$ adducts. Characterization data are given below for the complexes which could be isolated in analytically pure form. The solution equilibria involving these species are discussed below.

4-[(2,2,6,6-Tetramethyl-4-piperidyl-1-oxy)iminomethyl]pyridine–Copper Bis(hexafluoroacetylacetonate) Adduct (VII). Anhydrous $Cu(hfac)_2$, weighed under N_2, was dissolved in dry CCl_4. One equivalent of I dissolved in dry CCl_4 was added. The concentration of the final solution was ca. 0.10 M. The $Cu(hfac)_2$ solution immediately turned from purple to green, and a precipitate formed. The green precipitate was filtered in air and air-dried: yield 88%; IR $\nu_{C=N}$ 1640 cm^{-1}; $\mu_{eff} = 2.45$ μ_B (25 °C, $\chi^{dia} = -298.5 \times 10^{-6}$); vis (1:1

(2) Boymel, P. M.; Chang, J. R.; DuBois, D. L.; Greenslade, D. J.; Eaton, G. R.; Eaton, S. S. *J. Am. Chem. Soc.* **1977**, *99*, 5500–1.
(3) Braden, G. A.; Trevor, K. T.; Neri, J. M.; Greenslade, D. J.; Eaton, G. R.; Eaton, S. S. *J. Am. Chem. Soc.* **1977**, *99*, 4854–5.
(4) DuBois, D. L.; Eaton, G. R.; Eaton, S. S. *J. Am. Chem. Soc.* **1978**, *100*, 2686–9.
(5) DuBois, D. L.; Eaton, G. R.; Eaton, S. S. *Inorg. Chem.* **1979**, *18*, 75–9.
(6) DuBois, D. L.; Eaton, G. R.; Eaton, S. S. *J. Am. Chem. Soc.* **1979**, *101*, 2624–7.
(7) More, K. M.; Eaton, G. R.; Eaton, S. S. *Inorg. Chem.*, **1979**, *18*, 2492–6.
(8) The following abbreviations are used throughout the text: $Cu(hfac)_2$, bis(hexafluoroacetylacetonato)copper(II); py, pyridine; DTBN, di-*tert*-butyl nitroxide; bpy, 2,2′-bipyridyl; NO, a nitroxyl group; py~NO, a ligand which contains both a pyridine and a nitroxyl group; py~NR, a ligand which contains both a pyridine and a nitroxyl or piperidine amino group; ON~C=N–, a ligand which contains both a nitroxyl and an azomethine linkage; $Cu(hfac)_2$(N=C–), $Cu(hfac)_2$ bonded to an azomethine group; $Cu(hfac)_2$(>N–H), $Cu(hfac)_2$ bonded to a piperidine amino group; $Cu(hfac)_2$(>N–O), $Cu(hfac)_2$ bonded to a nitroxyl; $Cu(hfac)_2$(py~N—R), $Cu(hfac)_2$ bonded to the pyridine end of py~NR; $Cu(hfac)_2$(R—N~py), $Cu(hfac)_2$ bonded to the nitroxyl or piperidine amino group of R—N~py; $Cu(hfac)_2$(py~NR)$Cu(hfac)_2$, a dimer with one $Cu(hfac)_2$ bonded to the pyridine end and one $Cu(hfac)_2$ bonded to the nitroxyl or piperidine amino group of py~NR; ϵ, molar extinction coefficient at 775 nm; ϵ_{Cu}, ϵ for $Cu(hfac)_2$; ϵ_{py}, ϵ for $Cu(hfac)_2$py or $Cu(hfac)_2$(py~NR); $\epsilon_{(py)_2}$, ϵ for $Cu(hfac)_2(py)_2$ or $Cu(hfac)_2$(py~NR)$_2$; ϵ_{NO}, ϵ for $Cu(hfac)_2$(>NO); $\epsilon_{C=N}$, ϵ for $Cu(hfac)_2$(–N=C~).
(9) Gillard, R. D.; Wilkinson, G. *J. Chem. Soc.* **1963**, 5885–8.
(10) Brown, D. B.; Crawford, V. H.; Hall, J. W.; Hatfield, W. E. *J. Phys. Chem.* **1977**, *81*, 1303–6.
(11) Boudreaux, E. A., Mulay, L. N., Eds. "Theory and Applications of Molecular Paramagnetism"; Wiley: New York, 1976.
(12) Funck, L. L.; Ortolano, T. R. *Inorg. Chem.* **1968**, *7*, 567–73.

Table I. Equilibrium Constants and Extinction Coefficients[a] at 20 °C

ligand	K_1^{py}, M^{-1}	$10^{-2}K_2^{py}$, M^{-1}	$10^{-3}K_1^{NR}$, M^{-1}	K_{dimer}^{NR}, M^{-1}	ϵ_{py}, M^{-1} cm^{-1}	ϵ_{dimer}, M^{-1} cm^{-1}	ϵ_{NR}, M^{-1} cm^{-1}	ϵ_{dimer}, M^{-1} cm^{-1}
pyridine	$(7 \pm 5) \times 10^5$	7 ± 1			85 ± 2	25 ± 2		
DTBN			1.6 ± 0.4				295 ± 10	
py:DTBN[b]	$(6 \pm 2) \times 10^5$	7 ± 1	1.7 ± 0.2		85 ± 2	25 ± 2	295 ± 10	
XIV[c]			1.6 ± 0.4				205 ± 10	
XV			5.2 ± 0.4				167 ± 10	
I	$(6 \pm 2) \times 10^5$	4 ± 1	*d*	$(5.5 \pm 2) \times 10^2$	88 ± 1	25 ± 2	178 ± 15[e]	266 ± 15
II	$(6 \pm 2) \times 10^5$	4 ± 1	*d*	$(6.0 \pm 2) \times 10^2$	86 ± 1	27 ± 2	248 ± 20[e]	334 ± 20
III	$\geq 1 \times 10^7$ [f]		*d*	$(7.5 \pm 2) \times 10^2$	48 ± 1		158 ± 15[e]	206 ± 15
IV	$(6 \pm 2) \times 10^5$	7 ± 1	*g*	$(1.3 \pm 0.2) \times 10^3$	89 ± 1	27 ± 2	163 ± 10[e]	252 ± 10
V	$(6 \pm 2) \times 10^5$	4 ± 1	*g*	$(2.4 \pm 0.5) \times 10^3$	86 ± 1	27 ± 2	181 ± 10[e]	267 ± 10
VI	$\geq 1 \times 10^8$ [f]		*g*	$(2.5 \pm 0.5) \times 10^3$	46 ± 1		170 ± 10[e]	216 ± 5

[a] See text for definition of *K*'s and ε's. $\epsilon_{Cu} = 17 \pm 0.5$ M^{-1} cm^{-1}. [b] A competition study. [c] Assuming only the >N–O coordinates; see text. [d] Calculation is insensitive to the value of K_1^{NR} so K_1^{NR} was set equal to the value for ligand XIII. [e] Calculation is insensitive to the value of ϵ_{NR} due to low concentration of that species. The value given is based on the assumption that $\epsilon_{dimer} = \epsilon_{py} + \epsilon_{NR}$. [f] Since *K* is so large, only a lower limit on the value could be obtained. [g] Calculation is insensitive to the value of K_1^{NR} so K_1^{NR} was set equal to the value for ligand XIV.

mixture in CCl_4 at 20 °C) λ_{max} 750 nm (ε 90.4). Anal. Calcd for $C_{25}H_{24}CuF_{12}N_3O_5$: C, 40.69; H, 3.28; N, 5.69. Found: C, 40.58; H, 3.36; N, 5.64.

3-[(2,2,6,6-Tetramethyl-4-piperidyl-1-oxy)iminomethyl]pyridine–copper bis(hexafluoroacetylacetonate) adduct (VIII): yield 83%; IR $\nu_{C=N}$ 1645 cm^{-1}; $\mu_{eff} = 2.48$ μ_B (23 °C, $\chi^{dia} = -298.5 \times 10^{-6}$); vis (1:1 mixture in CCl_4 at 20 °C) λ_{max} 750 nm (ε 90.9). Anal. Calcd for $C_{25}H_{24}CuF_{12}N_3O_5$: C, 40.69; H, 3.28; N, 5.69. Found: C, 40.77; H, 3.16; N, 5.70.

2-[(2,2,6,6-Tetramethyl-4-piperidyl-1-oxy)iminomethyl]pyridine–Copper Bis(hexafluoroacetylacetonate) Adduct (IX). The yield was 87% (crude). The complex was recrystallized from CH_2Cl_2/hexane, giving olive green needles: IR $\nu_{C=N}$ 1665 cm^{-1}; $\mu_{eff} = 2.41$ μ_B (25 °C, $\chi^{dia} = -298.5 \times 10^{-6}$); vis (1:1 mixture in CCl_4 at 20 °C) λ_{max} 770 (ε 48.9). Anal. Calcd for $C_{25}H_{24}CuF_{12}N_3O_5$: C, 40.69; H, 3.28; N, 5.69. Found: C, 40.59; H, 3.12; N, 5.78.

2-[(2,2,6,6-Tetramethyl-4-piperidyl)iminomethyl]pyridine–Copper Bis(hexafluoroacetylacetonate) Adduct (XII). The yield was 93% (crude). The product was recrystallized from CH_2Cl_2/hexane: IR $\nu_{C=N}$ 1650 cm^{-1}; $\mu_{eff} = 1.74$ μ_B (25 °C, $\chi^{dia} = -304.1 \times 10^{-6}$); vis (1:1 mixture in CCl_4 at 20 °C) λ_{max} 770 (ε 46.4). Anal. Calcd for $C_{25}H_{25}CuF_{12}N_3O_4$: C, 41.53; H, 3.48; N, 5.81. Found: C, 41.24; H, 3.52; N, 5.68.

Computer Simulations. The EPR spectra were simulated by using the computer program CUNO which has been described previously.[7,13] The *g* values and hyperfine coupling constants for the nitroxyl ligands (I–III) and the copper complexes with diamagnetic ligands (X–XII) were used as starting parameters for simulation of the EPR spectra of the copper complexes with nitroxyl ligands (VII–IX).

Equilibrium Constants. For each type of equilibrium discussed below the equilibrium constant and mass-balance equations were solved to obtain an equation for the concentration of one species. The order of the equation was third order for $Cu(hfac)_2$ plus pyridine, fifth order for $Cu(hfac)_2$ plus pyridine plus di-*tert*-butyl nitroxide, and fifth order for $Cu(hfac)_2$ plus one of ligands I–VI. Interactive computer programs were written by using an IMSL[14] subroutine to find the roots of the higher order equations. The physically reasonable root was chosen by operator inspection and then used in the program to calculate the concentrations of all other species in the solution and to calculate the visible spectrum absorbance. Equilibrium constants and molar extinction coefficients were varied to obtain the best fit to the combined EPR and visible spectral data as discussed below. The uncertainties given for the values in Table I indicate the extent to which each parameter could be varied with compensating adjustments in other parameters while maintaining good agreement between calculated and observed absorbances (average discrepancy <0.003 A) and agreement within experimental uncertainty (uncertainty varies with concentration) between the calculated concentrations and the concentrations obtained from the EPR spectra.

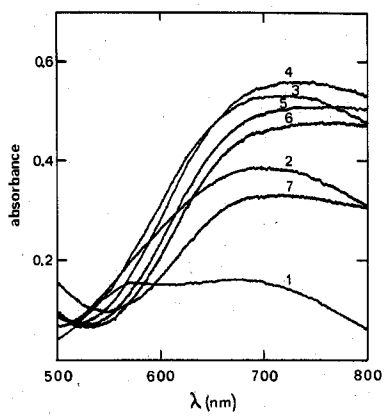

Figure 1. Visible spectra of 5.63×10^{-3} M $Cu(hfac)_2$ in the presence of various amounts of ligand I in CCl_4 at 20 °C. The ligand:metal ratios for the successive scans are (1) 0.0, (2) 0.25, (3) 0.50, (4) 0.75, (5) 1.0, (6) 1.1, and (7) 2.0.

Results and Discussion

Solution Equilibria. The visible spectra obtained when $Cu(hfac)_2$ was titrated with ligand I are presented in Figure 1. The absorbance at 775 nm reached a maximum at a ligand:$Cu(hfac)_2$ ratio of 0.75:1.0 and then decreased at higher ligand:metal ratios. There were also no isosbestic points in the spectra. Similar spectral changes were observed when $Cu(hfac)_2$ was titrated with ligands II–VI, except that for the potentially bidentate ligands III and VI, the spectra showed little additional change beyond ligand:metal ratios of 1:1. Clearly, more than two species are present in solution, indicating that coordination through the pyridine nitrogen to form a five-coordinate complex is not the only significant equilibrium. Since ligands I–VI each contain three potential donor sites (pyridine N, azomethine N, and nitroxyl O or piperidine N), studies were done on model complexes to ascertain the magnitude of the respective binding constants.

Funck and Ortolano[12] reported the titration of $Cu(hfac)_2$ with pyridine in CCl_4 and concluded that the visible spectra indicated the formation of both mono(pyridine) (eq 1) and bis(pyridine) (eq 2) adducts but did not report values of the

$$Cu(hfac)_2 + py \overset{K_1^{py}}{\rightleftharpoons} Cu(hfac)_2py \quad (1)$$

$$Cu(hfac)_2py + py \xrightarrow{K_2^{py}} Cu(hfac)_2(py)_2 \quad (2)$$

equilibrium constants. On the basis of thermodynamic studies, Drago and co-workers reported a value of $(3.4 \pm 0.9) \times 10^4$

(13) Eaton, S. S.; DuBois, D. L.; Eaton, G. R. *J. Magn. Reason.* **1978**, *32*, 251–63.

(14) International Mathematical and Statistical Libraries, Inc., Houston, TX 77036, IMSL Library 3, Edition 5 for the Burroughs 6700/7700 Computer, IMSL S-R032-E05.

for K_1^{py} in CH_2Cl_2[15] and a value of 570 ± 150 for K_2^{py} in CCl_4.[16] The EPR and visible spectra of a 5.11×10^{-3} M solution of $Cu(hfac)_2$ in CCl_4 were studied as a function of pyridine concentration from 1.28×10^{-3} M (0.25 equiv) to 2.55×10^{-2} M (9.0 equiv). The spectra were analyzed by using a computer program to solve the simultaneous equations for mono(pyridine) and bis(pyridine) adduct formation. The molar extinction coefficient for $Cu(hfac)_2$, ϵ_{Cu},[8] was taken from the spectrum in the absence of pyridine. The molar extinction coefficient of $Cu(hfac)_2(py)_2$, $\epsilon_{(py)_2}$, was taken from the spectrum of $Cu(hfac)_2$ in the presence of ~20-fold excess pyridine. The values of K_1^{py}, K_2^{py}, and the molar extinction coefficient of $Cu(hfac)_2py$, ϵ_{py}, were treated as adjustable parameters and varied iteratively to obtain the best agreement with the observed absorbance at 775 nm in our data and in the published spectra of Funck and Ortolano. Values of K's and ϵ's are summarized in Table I. The values obtained for K_1^{py} and K_2^{py} are in good agreement with the values reported previously by Drago et al.[15,16]

The g and A_{Cu} values for $Cu(hfac)_2$ and $Cu(hfac)_2py$ were sufficiently different that the highest field lines of the two species were well resolved in the EPR spectra. For ratios of pyridine:$Cu(hfac)_2$ up to 1:1, the concentration of $Cu(hfac)_2$ present in the mixture was obtained by subtraction of a spectrum of $Cu(hfac)_2$ from the spectrum of the mixture until the characteristic high-field line had been completely removed. The observed concentrations of $Cu(hfac)_2$ as a function of ligand added were in good agreement with the values predicted by K_1^{py} and K_2^{py} as obtained from the visible spectra.

It was reported previously that di-*tert*-butyl nitroxide (DTBN) coordinated to $Cu(hfac)_2$, but values of the equilibrium constant were not reported.[17] The visible spectra of 5.79×10^{-3} M $Cu(hfac)_2$ in CCl_4 were studied as a function of DTBN concentration for ligand:metal ratios from 0.25 to 5.0. The nitroxyl binding constant K_1^{NO} for equilibrium eq

$$Cu(hfac)_2 + >NO \xrightarrow{K_1^{NO}} Cu(hfac)_2(>NO) \quad (3)$$

3 was found to be $(1.6 \pm 0.4) \times 10^3$, and the molar extinction coefficient for $Cu(hfac)_2(>NO)$, ϵ_{NO}, was found to be 295 ± 10 (Table I). There was no indication of the formation of a six-coordinate complex. The value determined for K_1^{NO} is similar to the value of $(4.2 \pm 1.9) \times 10^3$ which was reported for the binding of 2,2,6,6-tetramethylpiperidinyl-1-oxy to $Cu(hfac)_2$ in cyclohexane at 25 °C.[18]

Since K_1^{py} is so large that there is considerable uncertainty in the value of K_1^{py} obtained from the visible spectra, a competition study was performed to check the relative values of K_1^{py} and K_1^{NO} for DTBN. The visible spectra of a 1:1 mixture of $Cu(hfac)_2$ and pyridine in CCl_4 were studied as a function of DTBN concentration. The spectra were analyzed by using a computer program to solve the simultaneous equilibria (1)–(3). The values of the equilibrium constants are in good agreement with the values obtained for the two ligands independently (Table I). Since ϵ_{NO} is substantially larger than ϵ_{py}, the calculated absorbance is very sensitive to the ratio of K_1^{NO} to K_1^{py}. As a result, the value of K_1^{py} obtained from this experiment is less uncertain than the value obtained directly.

The coordinating ability of the azomethine nitrogen was examined by using ligand XIII which was prepared by condensation of *p*-(trifluoromethyl)benzaldehyde with aminocyclohexane. Analysis of the visible spectra of $Cu(hfac)_2$ in

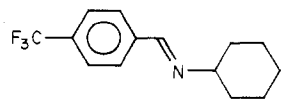

XIII

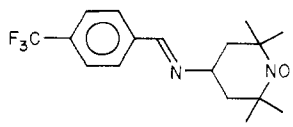

XIV

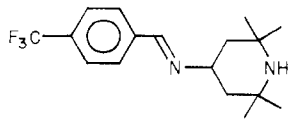

XV

CCl_4 as a function of added XIII, assuming (4), gave $K_1^{C=N}$

$$Cu(hfac)_2 + R{-}N{=}C{-} \xrightleftharpoons{K_1^{C=N}} Cu(hfac)_2(-N{=}C-) \quad (4)$$

$= 2.6 \times 10^2$ and the molar extinction coefficient of $Cu(hfac)_2(-N{=}C-)$, $\epsilon_{C=N}$, equal to 113 ± 2. There was no indication of the formation of a six-coordinate complex.

To further assess the relative coordinating abilities of the azomethine nitrogen and the nitroxyl oxygen, we examined ligand XIV. This ligand was prepared by condensation of *p*-(trifluoromethyl)benzaldehyde with 4-amino-2,2,6,6-tetramethylpiperidinyl-1-oxy. Since the ligand includes two donor sites the possibility of dimer formation, eq 5 and 6, was also

$$Cu(hfac)_2(ON\sim N{=}C) + Cu(hfac)_2 \xrightleftharpoons{K^{C=N}_{dimer}} Cu(hfac)_2(ON\sim N{=}C)Cu(hfac)_2 \quad (5)$$

$$Cu(hfac)_2(C{=}N\sim N{-}O) + Cu(hfac)_2 \xrightleftharpoons{K^{NO}_{dimer}} Cu(hfac)_2(ON\sim N{=}C)Cu(hfac)_2 \quad (6)$$

examined. The visible spectra of $Cu(hfac)_2$ in CCl_4 in the presence of varying amounts of XIV were satisfactorily interpreted in terms of a single binding constant, $K = 1.6 \times 10^3$, and ϵ for the mono adduct is 205 ± 10. The similarity of the value of K to that of K_1^{NO} for DTBN indicated that the predominant binding of ligand XIV is through the nitroxyl oxygen, eq 3. The value of $K_1^{C=N}$ (eq 4) was not well-defined by the visible spectra due to the much larger value of K_1^{NO}. Values of $K_1^{C=N}$ (eq 4) from 0 to 1.0×10^2 were consistent with the observed data. However, to fit the data, $K_{dimer}^{C=N}$ (eq 5) must be <15, indicating that the azomethine nitrogen does not participate significantly in dimer formation.

Ligand XV, also prepared by a Schiff base condensation, was studied to determine the binding constant for the piperidine nitrogen. The visible spectra of $Cu(hfac)_2$ in CCl_4 as a function of the concentration of ligand XV added were fit with a single equilibrium constant (eq 7) with $K_1^{NH} = (5.2 \pm 0.4) \times 10^3$ and ϵ_{NH} 167 ± 10. It was not necessary to include equilibrium 4 or dimer formation to fit the data.

$$Cu(hfac)_2 + >N{-}H \xrightleftharpoons{K_1^{NH}} Cu(hfac)_2(>N{-}H) \quad (7)$$

Comparison of the observed binding constants for model compounds containing donor sites analogous to those in ligands I–VI indicated that the equilibrium constants fall in the order $K_1^{py} >> K_1^{NH} > K_1^{NO} > K_1^{C=N}$. Since K_1^{py} was at least 2 orders of magnitude greater than any of the other binding constants in the system, the predominant monomeric five-coordinate species would be formed by coordination of the pyridine nitrogen. However the substantial coordinating ability of the nitroxyl oxygen and the piperidine amino groups could result in dimer formation. Since the data on ligand XIV indicated that the azomethine nitrogen did not participate significantly in dimer formation, its contribution was assumed to be negligible in the equilibria involving ligands I–VI. Therefore the equilibria of ligands I–VI were analyzed in terms of eq 8–12 with N–R representing N–O or NH. The two

(15) McMillin, D. R.; Drago, R. S.; Nusz, J. A. *J. Am. Chem. Soc.* **1976**, *98*, 3120–6.
(16) Partenheimer, W.; Drago, R. S. *Inorg. Chem.* **1970**, *9*, 47–52.
(17) Zelonka, R. A.; Baird, M. C. *Chem. Commun.* **1970**, 1148. Zelonka, R. A.; Baird, M. C. *J. Am. Chem. Soc.*, **1971**, *93*, 6066–70.
(18) Lim, Y. Y.; Drago, R. S. *Inorg. Chem.* **1972**, *11*, 1334–8.

Table II. EPR Spectra of Complexes with Diamagnetic Ligands

complex[a]	solvent[b]	g_{iso}[c,d]	A_{Cu},[c,e] G	A_N,[c,f] G	$g_\parallel$[g,h]	$A_\parallel^{Cu}$,[g,i] G	A[c,j]	B[c,j]	C[c,j]
$Cu(hfac)_2$	CCl_4	2.1334	69.8				26.8	9.1	0.7
$Cu(hfac)_2$	toluene	2.1331	68.0		2.285	170	28.7	6.7	0.8
$Cu(hfac)_2$·IV	CCl_4	2.1502	51.0	11.0[k]			31.5	13.2	2.0
$Cu(hfac)_2$·IV	toluene	2.1482	53.0	11.0[k]	2.295	140	29.2	12.1	2.2
$Cu(hfac)_2$·V	CCl_4	2.1512	51.0	11.0[k]			30.1	11.3	1.6
$Cu(hfac)_2$·V	toluene	2.1496	53.0	11.0[k]	2.310	140	29.1	10.6	1.7
$Cu(hfac)_2$·VI	CCl_4	2.1566	42.0	12.0[l]			44.7	12.3	3.3
$Cu(hfac)_2$·VI	toluene	2.1548	43.2	11.5[l]	2.306	150	42.3	8.6	2.2
$Cu(hfac)_2$·XV	CCl_4	2.1567	48.0	10.0[k]			36.6	15.1	1.8

[a] All spectra were taken at 20 or −196 °C on samples with a 1:1 ratio of $Cu(hfac)_2$:ligand except for $Cu(hfac)_2$·XV which was taken in the presence of a fivefold excess of ligand to maximize complex formation. [b] Concentrations were 5×10^{-3} M for toluene solutions and 1.0×10^{-2} M for CCl_4 solutions. [c] Based on computer simulations. [d] Uncertainty ±0.0007 G. [e] Uncertainty ±0.5 G; values are for ^{63}Cu. [f] Uncertainty ±2.0 G. [g] Estimated directly from frozen spectra. [h] Uncertainty ±0.005 G. [i] Uncertainty ±5 G; values for ^{63}Cu. [j] Line width parameters; see text. [k] One equivalent nitrogen. [l] Two equivalent nitrogens.

equilibrium constants for dimer formation are not independent variables and are related by $K_{dimer}^{py} = K_{dimer}^{NR} K_1^{py} / K_1^{NO}$.

$$Cu(hfac)_2 + py\sim N{-}R \overset{K_1^{py}}{\rightleftharpoons} Cu(hfac)_2(py\sim N{-}R) \quad (8)$$

$$Cu(hfac)_2 + py\sim N{-}R \overset{K_1^{NO}}{\rightleftharpoons} Cu(hfac)_2(R{-}N\sim py) \quad (9)$$

$$Cu(hfac)_2(py\sim N{-}R) + py\sim N{-}R \overset{K_2^{py}}{\rightleftharpoons} Cu(hfac)_2(py\sim N{-}R)_2 \quad (10)$$

$$Cu(hfac)_2(py\sim N{-}R) + Cu(hfac)_2 \overset{K^{NR}_{dimer}}{\rightleftharpoons} Cu(hfac)_2(py\sim NR)Cu(hfac)_2 \quad (11)$$

$$Cu(hfac)_2(R{-}N\sim py) + Cu(hfac)_2 \overset{K^{py}_{dimer}}{\rightleftharpoons} Cu(hfac)_2(py\sim NR)Cu(hfac)_2 \quad (12)$$

Visible and EPR spectra of $Cu(hfac)_2$ in CCl_4 in the presence of ligands I–VI were recorded with ligand:metal ratios from 0.25:1.0 to 5.0:1.0. The equilibrium constants were obtained by fitting the data from both the EPR and visible spectra. For the complexes with diamagnetic ligands, IV–VI, the concentration of $Cu(hfac)_2$ in each sample was obtained by subtraction of an EPR spectrum of $Cu(hfac)_2$ from the EPR spectrum of each mixture. For the complexes with nitroxyl ligands I–III, the EPR spectra of the various species overlapped too much to allow the concentration of $Cu(hfac)_2$ to be determined accurately by subtraction. However, when Cu is bound directly to the nitroxyl oxygen, the complex is strongly antiferromagnetically coupled[17,18] and there is no observable EPR signal at room temperature. Therefore the difference between the expected integrated intensity of the EPR spectrum at a particular ligand:metal ratio and the observed integrated intensity was used to estimate the dimer concentration. For each ligand, the equilibrium constants and molar extinction coefficients were iteratively varied to obtain the best agreement with both the visible spectra and the EPR data. The calculations were very insensitive to the values used for K_1^{NR} and ϵ_{NR} because of the low concentration of this species in the equilibrium mixture. Therefore K_1^{NR} was set equal to the value observed for the corresponding model compound and ϵ_{NR} was assumed to be equal to $\epsilon_{dimer} - \epsilon_{py}$; i.e. it was assumed that the absorbance of the dimer was due to two independent copper centers. With these assumptions the values given in Table I were obtained. In all cases the calculated absorbances and concentrations (from EPR) were in good agreement with the experimental values.

The absorption spectra in Figure 1 can thus be explained as follows. At low ligand concentrations there is a significant amount of dimer present, and since $\epsilon_{NO} > \epsilon_{py} > \epsilon_{Cu}$, there is an increase in the absorption. The dimer formation is greatest at a I:$Cu(hfac)_2$ ratio of 0.5:1.0. At higher ligand concentrations the dimer formation decreases because the nitroxyl oxygen is displaced by the stronger donor pyridine and the absorption decreases because $\epsilon_{py} < \epsilon_{NO}$. At ligand:metal ratios near 1:1 $Cu(hfac)_2$·I is the primary species in solution. Then as excess ligand is added, the concentration of the six-coordinate complex with two coordinated pyridines increases and the absorbance drops because $\epsilon_{(py)_2} < \epsilon_{py}$. Figure 2 depicts the concentrations of the various copper containing species in solution as a function of added ligand when 5.63×10^{-3} M $Cu(hfac)_2$ is titrated with ligand I. Concentrations are based on the equilibrium constants in Table I. For a 1:1 mixture the copper present in the various species expressed as a percent of total copper concentration is as follows: $Cu(hfac)_2$, 1.4; $Cu(hfac)_2(py\sim NO)$, 87.0; $Cu(hfac)_2(NO\sim py)$, 0.3; $Cu(hfac)_2(py\sim NO)_2$, 3.5; $Cu(hfac)_2(py\sim NO)Cu(hfac)_2$, 7.7; (py–NO), 1.8 (relative to total copper). Thus despite the fact that K_1^{py} is very large and appreciably greater than any of the other equilibrium constants, the concentrations of species other than the 1:1 adduct are significant. Therefore these other species were taken into consideration in analyzing the EPR spectra. Given the complexity of the equilibrium it is also not surprising that in two cases (ligands IV and V) it was not possible to isolate the 1:1 adducts in analytically pure form.

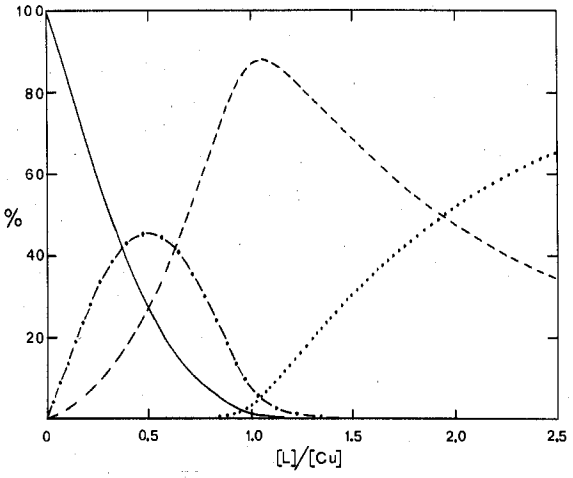

Figure 2. The composition of the equilibrium mixture of 5.63×10^{-3} M $Cu(hfac)_2$ and ligand I as a function of the ligand:metal ratio. Concentrations are expressed as percentages of the total copper present: —, $Cu(hfac)_2$; - - -, $Cu(hfac)_2(NO\sim py)Cu(hfac)_2$; - - -, $Cu(hfac)_2$·I; ···, $Cu(hfac)_2$·I_2. Curves were calculated by using the equilibrium constants in Table I.

For ligands I–III there were further color changes and/or precipitation indicative of additional species at very high ligand:metal ratios (>5:1). The nature of these complexes was not explored.

The values obtained for the equilibrium constants for ligands I–VI are similar to those obtained for the model compounds

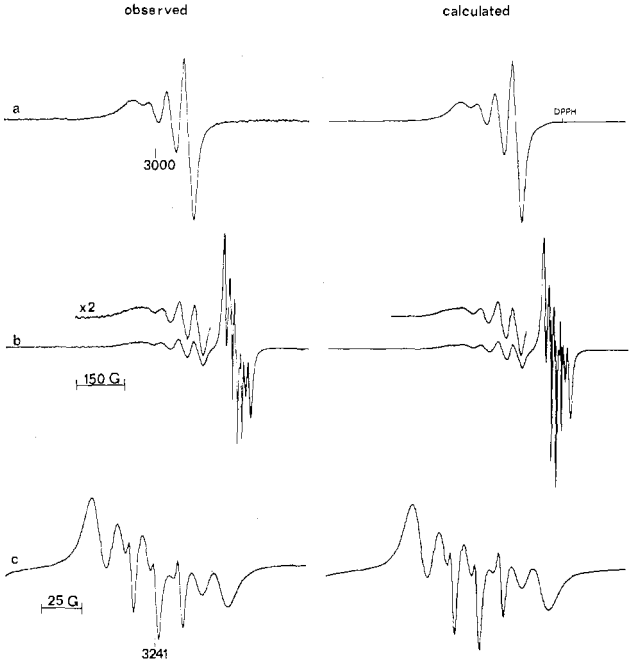

Figure 3. X-Band EPR spectra in CCl_4 at 20 °C and computer simulations: (a) $Cu(hfac)_2$·IV, 1000-G scan, 125-G/min scan rate, 5 mW, 0.40-G modulation amplitude; (b) $Cu(hfac)_2$·I, 1000-G scan, 125-G/min scan rate, 5 mW, 0.40-G modulation amplitude; (c) 200-G scan of nitroxyl region of (b), 25-G/min scan rate, 5 mW, 0.40-G modulation amplitude. Parameters for simulated spectra are given in Tables II and III.

pyridine, DTBN, XIV, and XV (Table I). The values of K_1^{py} for the monodentate ligands I, II, IV, and V are within experimental error of the values obtained for pyridine. The value of K_1^{py} is larger for the bidentate ligands III and VI than for the monodentates. The binding constants for dimer formation through the nitroxyl or piperidine amino groups (K_{dimer}^{NR}) are a factor of 2 to 3 lower than the binding constants for the respective groups in the model compounds. This may reflect differences in steric hindrance or solvation. The molar extinction coefficients calculated for the complexes are also quite similar to those obtained for the model complexes.

EPR Spectra. The room-temperature solution EPR spectra of the $Cu(hfac)_2$ adducts with the diamagnetic ligands IV, V, VI, and XV showed the typical four-line patterns expected for coupling of the electron to the spin $^3/_2$ copper(II) nucleus. The spectra of $Cu(hfac)_2$·IV and $Cu(hfac)_2$·VI are shown in Figures 3a and 4a, respectively, and the parameters obtained by computer simulation of the spectra are given in Table II. The values we obtained for $Cu(hfac)_2$ are included in Table II and are in good agreement with recent literature values.[19] These values were used in simulating the $Cu(hfac)_2$ component of the equilibrium mixtures with all of the diamagnetic and paramagnetic ligands. The equilibrium calculations for the $Cu(hfac)_2$ adducts of ligands IV and V indicated the presence of 13.3 and 15.3% dimer, respectively, in the 1:1 mixture. It was assumed that the EPR spectrum for the dimer would be the sum of the spectra of $Cu(hfac)_2$py and $Cu(hfac)_2$·XV. However, the A_{Cu} and g values of these species are so similar to those of the adducts of IV and V that inclusion of the appropriate concentrations of dimer in the simulations of the EPR spectra of $Cu(hfac)_2$·IV and $Cu(hfac)_2$·V had no observable impact on the appearance of the spectra. The binding constant for the bidentate ligand VI is so large that there is a negligible dimer concentration at a 1:1 ligand:metal ratio.

(19) Yokoi, H. *Inorg. Chem.* **1978**, *17*, 538–42.

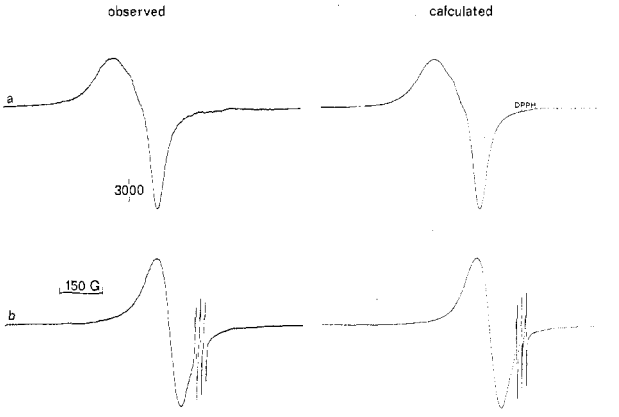

Figure 4. X-Band EPR spectra in CCl_4 at 20 °C and computer simulations: (a) $Cu(hfac)_2$·VI, 1000-G scan, 125-G/min scan rate, 5 mW, 2.5-G modulation amplitude; (b) $Cu(hfac)_2$·III, 1000-G scan, 125-G/min scan rate, 5 mW, 2.5-G modulation amplitude. Parameters for simulated spectra including the concentrations of species which contribute are given in Tables II and III. The triplet in (b) is due to a small amount of uncoordinated nitroxyl in the equilibrium mixture.

The contributions of the dimers to the EPR spectra were therefore ignored. In order to obtain good agreement between the observed and calculated spectra it was necessary to include superhyperfine coupling to the pyridine nitrogen in $Cu(hfac)_2$·IV and $Cu(hfac)_2$·V and to the pyridine and azomethine nitrogens in $Cu(hfac)_2$·VI. Values of A_N between 11.0 and 12.0 G (Table II) were found to give the best fit to the experimental spectra. These values are in good agreement with the values of A_N reported previously for $Cu(hfac)_2$py,[15] $Cu(hfac)_2(py)_2$,[20] and $Cu(hfac)_2$bpy.[21]

The EPR spectra of $Cu(hfac)_2$·IV, $Cu(hfac)_2$·V, and $Cu(hfac)_2$·VI were also obtained in frozen toluene solutions. Values of $A_{\parallel}^{Cu}$ and $g_{\parallel}$ were estimated from the spectra (Table II). The perpendicular components were not resolved in any of the spectra. The values of $A_{\parallel}$ and $g_{\parallel}$ for $Cu(hfac)_2$·IV and $Cu(hfac)_2$·V are very similar to those reported for $Cu(hfac)_2$py.[15] $g_{\parallel}$ is greater than $g_{\perp}$ as is commonly observed for square-pyramidal copper complexes.[15] The values of $g_{\parallel}$ and $A_{\parallel}$ observed for $Cu(hfac)_2$·VI are within experimental error of the parameters reported for $Cu(hfac)_2(bpy)$[21,22] which has been shown by X-ray crystallography to have a distorted octahedral geometry with bipyridyl occupying cis equatorial positions.[21]

As shown in Figure 3b,c the EPR spectra of $Cu(hfac)_2$·I are clearly an example of electron–electron coupling as indicated in the preliminary communication of this work.[2] The "nitroxyl" region of the spectrum is a doublet of triplets, and, although less clearly resolved, the "copper" region is a doublet of quartets. Simulation of the spectra using the computer program CUNO[13] produced the spectra given on the right-hand side of the figure using a value of 43.5 G for the spin–spin coupling constant, J (Table III). The three sharp lines in the center of the "nitroxyl" region are due to nitroxyl which is not interacting with a copper which will subsequently be referred to as "free" nitroxyl. The equilibrium calculations indicated the presence of dimer $Cu(hfac)_2$(py⁓NO)$Cu(hfac)_2$ in the 1:1 mixture. It was assumed that the EPR spectra of the dimer would be the superposition of the spectra of $Cu(hfac)_2$py and $Cu(hfac)_2$NO, but since the spins in $Cu(hfac)_2$NO are strongly antiferromagnetically coupled,[17,18] that portion of the dimer made no contribution to the EPR spectra. The simulated

(20) Pradillo-Sorzano, J.; Fackler, J. P., Jr. *Inorg. Chem.* **1973**, *12*, 1182–9.
(21) Veidis, M. V.; Schreiber, G. H.; Gough, T. E.; Palenik, G. J. *J. Am. Chem. Soc.* **1969**, *91*, 1859–60.
(22) Dudley, R. J.; Hathaway, B. J. *J. Chem. Soc. A* **1970**, 2794–9.

Table III. EPR Spectra of Complexes with Paramagnetic Ligands[a]

complex	J,[a] G	J, cm^{-1}	Cu parameters					% soln compn copper species[h]			
			g_{iso}[a,b]	A_{Cu},[a,c] G	A_N,[a,d] G	$g_\parallel$[e,f]	$A_\parallel^{Cu}$,[e,g] G	1:1 adduct	$Cu(hfac)_2$	dimer	free nitroxyl
$Cu(hfac)_2$·I	43.5	4.22×10^{-3}	2.1529	52.5	11.0	2.285	140	87.0	1.4	7.7	3.8
$Cu(hfac)_2$·II											
isomer I	37.0	3.58×10^{-3}	2.1402	56.0	5.5[i]	2.250	140	52.2	1.4	7.9	2.3
isomer II	94.0	9.11×10^{-3}	2.1523	49.0	11.0	2.352	152	34.8			
$Cu(hfac)_2$·III	>1000	$>9.7 \times 10^{-2}$	2.1566	42.0	12.0	[j]		100	0	0	0.75

[a] Obtained by computer simulation of EPR spectra of 1:1 mixture of $Cu(hfac)_2$ and ligand in CCl_4 at 20 °C. Nitroxyl parameters: g = 2.0062, A_N = 15.3 ± 0.26. [b] Uncertainty ±0.0007. [c] Uncertainty ±1.0 G; value for ^{63}Cu. [d] Uncertainty ±1.0 G unless otherwise noted. [e] Taken directly from spectra of frozen toluene solutions. [f] Uncertainty ±0.005. [g] Uncertainty ±5.0 G. [h] Percent of total copper concentration present in each species based on equilibrium constants from Table I and used in simulations. The concentration of free nitroxyl (relative to total copper) is the value adjusted to fit the observed spectra and differs slightly from the value based on the equilibrium constants. $Cu(hfac)_2(py{\sim\sim}NO)_2$ is about 3.5% of the total Cu; this species was not included in the simulations. [i] This value is highly uncertain since spectra were insensitive to substantial changes in A_N. [j] Single averaged line observed at g = 2.068.

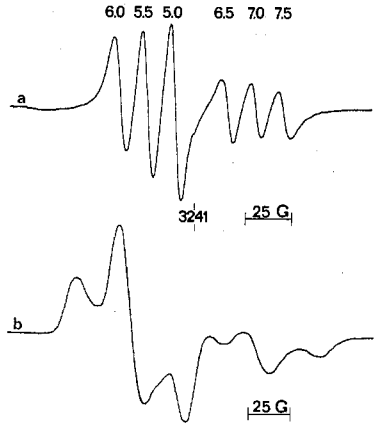

Figure 5. (a) Nitroxyl region of the X-band EPR spectrum of $Cu(hfac)_2$·I in toluene at −45 °C. The numbers above the lines are the line widths obtained by computer simulation: 200-G scan, 25-G/min scan rate, 2 mW, 0.16-G modulation amplitude. (b) Nitroxyl region of the X-band EPR spectrum of $Cu(hfac)_2$·I in frozen toluene solution: 220-G scan, 125-G/min scan rate, 2 mW, 0.40-G modulation amplitude.

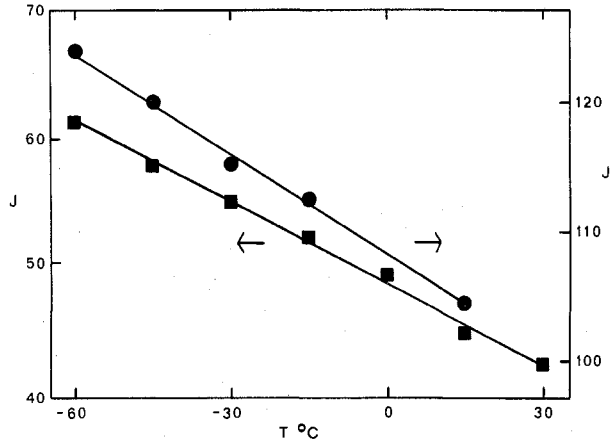

Figure 6. Temperature dependence of the electron–electron coupling constant, J, in gauss in $Cu(hfac)_2$·I (■) and in isomer II of $Cu(hfac)_2$·II (●) in toluene solution.

spectra included contributions from $Cu(hfac)_2$ and dimer as calculated from the equilibrium constants in Table I. The agreement between calculated and observed spectra of the "copper" region was improved by inclusion of all species.

As the temperature was decreased, the tumbling rate of the molecule decreased and the "copper" region of the spectrum became difficult to interpret while the "nitroxyl" region

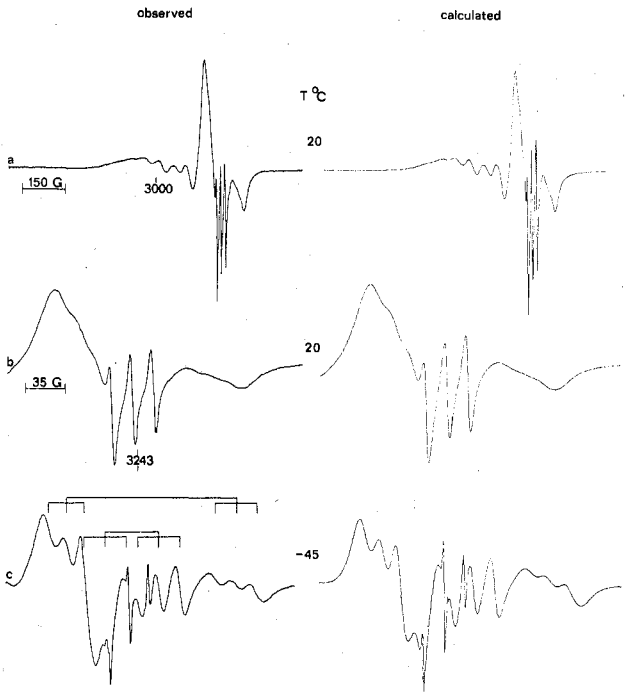

Figure 7. X-Band EPR spectra and computer simulations: (a) $Cu(hfac)_2$·II in CCl_4 at 20 °C, 1000-G scan, 125-G/min scan rate, 5 mW, 0.32-G modulation amplitude; (b) 200-G scan of the nitroxyl region from (a), 50-G/min scan rate, 5 mW, 0.32-G modulation amplitude; (c) nitroxyl region of the spectrum of $Cu(hfac)_2$·II in toluene at −45 °C, 200-G scan, 50-G/min scan rate, 2 mW, 0.40-G modulation amplitude. The bars indicate the positions of the doublet of triplets for the two isomers. Parameters for the simulated spectra are given in Tables II and III.

sharpened. At −45 °C (Figure 5a) the nitroxyl line widths for the "inner" lines decreased to higher field whereas the "outer" line widths increased to higher field. Similar nitroxyl line width variation has been observed for spin-labeled copper salicylaldimines,[7] and the interpretation of the line widths is currently under investigation. In addition the value of J was found to increase with decreasing temperature as plotted in Figure 6.

The EPR spectrum of $Cu(hfac)_2$·I in frozen toluene solution also showed the splitting of the nitroxyl signals due to electron–electron coupling (Figure 5b). The two patterns typical of immobilized nitroxyls were separated by about 71 G which is very similar to the values of J obtained in solution. The copper lines were too broad to observe the 71-G splitting and looked very similar to the signals observed for the analogous complex with a diamagnetic ligand, $Cu(hfac)_2$·IV.

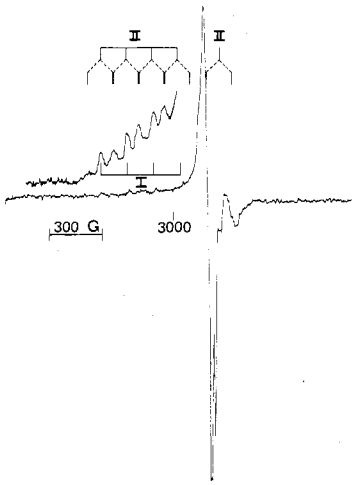

Figure 8. X-Band EPR spectrum of $Cu(hfac)_2$·II in frozen toluene solution. Markings denote positions of $g_{\|}$ lines for isomer I and positions of "inner" and "outer" $g_{\|}$ lines and "inner" and "outer" nitroxyl lines for isomer II: 2000-G scan, 250-G/min scan rate, 2 mW, 2.0-G modulation amplitude. The insert showing details of the $g_{\|}$ region is amplified 10 times the full spectrum.

The room-temperature EPR spectra of $Cu(hfac)_2$·II in CCl_4 solution are shown in Figure 7a,b. Although the room temperature "nitroxyl" region is poorly resolved, the simulations indicated that it is a mixture of two isomers denoted I and II with values of J = 37 and 94 G, respectively. The presence of the two isomers can be seen more clearly at −45 °C in toluene solution (Figure 7c). Simulations of the nitroxyl region of the spectrum at −45 °C gave values of J for isomers I and II as 37 and 120 G, respectively, although the slowing of the molecular tumbling made it difficult to interpret the copper region of the spectrum. To provide comparison with the other complexes, we based the values in Table III on simulations at 20 °C. The larger line widths for the nitroxyl lines at room temperature made it difficult to assess the populations of the two isomers. The relative concentrations of isomers I and II were varied in a series of simulations. Reasonably good agreement between calculated and observed spectra could be obtained with ratios of isomer I:isomer II of 70:30 and 50:50 with compensating changes in line width parameters. However the best agreement was at 60:40, and these ratios are used in the simulated spectra appearing in Figure 7. Concentrations of $Cu(hfac)_2$ and $Cu(hfac)_2(py{\sim}NO)Cu(hfac)_2$ based on the equilibrium constants in Table I were also included. The dimer was treated as in the case of $Cu(hfac)_2$·I.

As the temperature was decreased, the value of J for isomer I remained essentially constant while the value of J for isomer II increased as plotted in Figure 6. The relative concentrations of the two species did not change significantly over the temperature ranges examined. Studies at higher temperatures were precluded by extensive dissociation of the adduct. The spectrum of $Cu(hfac)_2$·II in frozen toluene solution also indicated the presence of two isomers with partially resolved lines as indicated in Figure 8. On the basis of the splitting between the lowest field pair of inner and outer "copper" lines and the splitting of the nitroxyl lines, the value of J for isomer II is about 150 G. (The value of J in fluid toluene solutions ranged from 104 to 124 G, dependent on temperature.) The other "outer" copper lines for isomer II are superimposed on the more intense "inner" copper lines because $A_{\|}^{Cu}$ and J have very similar values. The lines assigned to isomer I are sufficiently broad that a value of J of about 40 G, as observed in solution, would not be resolved. The highest field $g_{\|}$ copper lines for isomers I and II are partially superimposed on the $g_{\perp}$ copper lines and on the nitroxyl region of the spectrum. The nature of the two isomers is not known.

The EPR spectra of $Cu(hfac)_2$·III (Figure 4b) consist of a single broad line with a g value which is the average of the g values for $Cu(hfac)_2$·VI and for free nitroxyl, indicating a strong electron–electron interaction. Even when high power and gain settings were used, no "outer" lines were found. We have previously detected "outer" nitroxyl lines for a complex with J = 2650 G,[6] but if the line widths for the outer lines were greater in the present case, it might be more difficult to detect the lines. Simulations indicated that J must be greater than 1000 G to obtain a fully averaged line. The spectrum of $Cu(hfac)_2$·III in frozen toluene solution was a single line centered at the field expected for a signal with a g value which is the average of g values for copper and nitroxyl, consistent with a large value of J. EPR parameters are summarized in Table III.

The EPR spectra of the $Cu(hfac)_2$ adducts of ligands I–III show electron–electron coupling constants in the range of 37.0–>1000 G at room temperature in CCl_4 solution. Two isomers were observed for $Cu(hfac)_2$·II. Two isomers have been reported for $Cu(hfac)_2$(tetrahydrothiophene)[15] and for $Cu(hfac)_2$(triphenylphosphine)[23] and were attributed to coordination of the fifth ligand to axial and basal sites in square-pyramidal complexes.[15,23] However there is also the possibility of distorted geometries. Bencini et al. have recently reported the EPR spectra for two complexes which have geometries intermediate between trigonal bipyramidal and square pyramidal.[24] The overall appearance of the published EPR spectra of these complexes and the $g_{\|}$ and $A_{\|}$ values are quite similar to those obtained in this study. The information available for isomers I and II of $Cu(hfac)_2$·II does not provide an adequate basis for structure assignment. There are many feasible structures which one could speculate for the two isomers in $Cu(hfac)_2$·II. However it is not obvious how such speculations could be tested. The similarity of the EPR parameters (Table III) for the two isomers and for $Cu(hfac)_2$·I indicates that the copper ligand coordination is similar for the three complexes. Detailed interpretation of the differences in J for $Cu(hfac)_2$·I and $Cu(hfac)_2$·II cannot be made without structural information. However, the values of J for these three complexes are all significantly smaller than the value of J for $Cu(hfac)_2$·III. Thus when the nitroxyl is moved substantially closer to the copper, the value of J increases.

The value of J increased with decreasing temperature for $Cu(hfac)_2$·I and isomer II of $Cu(hfac)_2$ as shown in Figure 6. A similar increase in J with decreasing temperature was observed for spin-labeled Cu(baen),[6] but in one spin-labeled copper salicylaldimine the value of J decreased with decreasing temperature[7] and in another spin-labeled copper salicylaldimine the value of J was essentially independent of temperature.[7] The value of J for isomer I of $Cu(hfac)_2$·II was also insensitive to temperature changes. Further studies are required to interpret the differences in temperature-dependent behavior.

The similarities between the electron–electron coupling constants observed in fluid solution and frozen solution for both $Cu(hfac)_2$·I and $Cu(hfac)_2$·II are particularly striking results. Commonly it is assumed that electron–electron interactions in rigid media are purely dipolar, and electron–electron distances have been calculated from the spectral splittings.[1] For the case of interacting spins tumbling rapidly in solution, our best estimate is that dipolar splittings will be small (probably less than the line widths we observe) even for the anisotropic and nonequivalent g factors involved in the complexes reported herein. Further work is necessary in this area. However it

(23) Wayland, B. B.; Kapur, V. K. *Inorg. Chem.* **1974**, *13*, 2517–20.
(24) Bencini, A.; Bertini, I.; Gatteschi, D.; Scozzafava, A. *Inorg. Chem.* **1978**, *17*, 3194–7.

appears that the room-temperature-solution EPR data are reasonably interpreted as a measure of exchange interactions. The values of J measured from frozen-solution spectra did not correspond to linear extrapolation of fluid-solution data, but there is no reason to expect them to correspond to the extrapolation, although the values are similar. Interpretation of the frozen-solution EPR splitting as pure dipolar interactions permits calculation of a copper–nitroxyl distance using the simple point-dipole formula for nonequivalent spins[25,26] $r = (2g\beta/|2D|)^{1/3}$, where $|2D|$ denotes the observed splitting. If the observed splittings in the frozen-solution spectra of Cu(hfac)$_2$·I and Cu(hfac)$_2$·II were assumed to be purely dipolar, then the calculated copper–nitroxyl distances would be 8.1 and 6.3 Å, respectively. However, using CPK molecular models and assuming various molecular conformations which seemed reasonably strain free, we estimated copper–nitroxyl distances of 12 and 10 Å, respectively. At these distances the calculated dipolar couplings would be 22 and 37 G, respectively. Although the calculated numbers are very approximate, they are probably reasonable estimates for the upper limits on the dipolar contribution to the coupling. Even if the molecules were to adopt rather different conformations, it appears unlikely that the dipolar contributions could be greater than half the observed splittings.[27] Consequently considerable caution must be exercised in attributing all splittings in frozen solution to dipolar coupling and in assuming that the splitting can be used to calculate metal–nitroxyl distances in rigid-media spectra.

Acknowledgment. Elemental analyses were performed by Spang Microanalytical Laboratory and Galbraith Analytical Laboratory. This work was supported in part by the National Institutes of Health (Grant GM 21156) and a Marathon Summer Research Fellowship (P.M.B.). Discussions with coauthors of prior papers in this series contributed to this paper.

Registry No. I, 64013-19-0; II, 72442-95-6; III, 72453-28-2; IV, 72442-96-7; V, 72442-97-8; VI, 72442-98-9; VII, 64071-78-9; VIII, 72057-28-4; IX, 72442-72-9; X, 72442-73-0; XI, 72442-74-1; XII, 72442-75-2; Cu(hfac)$_2$·XIV, 72442-76-3; Cu(hfac)$_2$·XV, 72442-77-4; Cu(hfac)$_2$(py)$_2$, 38496-50-3; Cu(hfac)$_2$(DTBN), 35164-63-7; Cu(hfac)$_2$, 14781-45-4; 4-amino-2,2,6,6-tetramethylpiperidinyl-1-oxy, 14691-88-4; pyridine-4-carboxaldehyde, 872-85-5; pyridine-3-carboxaldehyde, 500-22-1; pyridine-2-carboxaldehyde, 1121-60-4; Cu(hfac)$_2$·XIII, 72442-78-5.

(25) Poole, C. P., Jr. "Electron Spin Resonance"; Wiley-Interscience: New York, 1967; p 822.
(26) Jost, P.; Griffith, O. H. In "Methods in Pharmacology"; Chignell, C., Ed.; Appleton-Century-Crofts: New York, 1971; Vol. II, p 242.
(27) It should also be noted that the sign of J is not known.

Contribution from the Departments of Chemistry, University of Denver, Denver, Colorado 80208, and the University of Colorado at Denver, Denver, Colorado 80202

Metal–Nitroxyl Interactions. 17. Spin-Labeled Adducts of Bis(hexafluoroacetylacetonato)copper(II)

P. M. BOYMEL, G. A. BRADEN, G. R. EATON,* and S. S. EATON

Received August 27, 1979

Spin-labeled ligands have been prepared by condensing pyridine-4-carboxaldehyde, pyridine-3-carboxaldehyde, and pyridine-2-carboxaldehyde with 3-amino-2,2,5,5-tetramethylpyrrolidinyl-1-oxy and by condensing pyridine-4-carboxaldehyde with 3-aminomethyl-2,2,5,5-tetramethylpyrrolidinyl-1-oxy. The equilibrium constants have been obtained for the coordination of these ligands to bis(hexafluoroacetylacetonato)copper(II) in CCl_4 at 20 °C. The EPR spectra of the 1:1 complexes exhibit electron–electron coupling in CCl_4 at room temperature with values of the coupling constant ranging from ca. 30 to >2000 G.

Introduction

The utility of the spin-label and spin-probe techniques in the study of biological systems has generated substantial interest in the interactions which may occur if a metal ion is present in the spin-labeled system.[1] We have demonstrated that in a variety of copper complexes with ligands which contain nitroxyl radicals, electron spin–electron spin coupling is observed in the room-temperature solution EPR spectra.[2-5] Values of the coupling constant, J, ranging from 4.8[4] to >2650 G[2] have been found. We have recently reported equilibria and EPR studies of the interaction of the homologous series of spin-labeled pyridines (I–III) with Cu(hfac)$_2$.[5,6] Values of J from 37.0 to >1000 G were observed. In order to elucidate the effect of the nitroxyl ring size on J, we now report analogous studies with the spin-labeled pyridines IV–VI. To explore the effect of the linkage between the pyridine and nitroxyl rings, we examined ligand VII.

Experimental Section

Physical Measurements. Infrared spectra were obtained in halocarbon and Nujol mulls on a Perkin-Elmer 337 grating spectrometer. Magnetic susceptibilities were measured on a Bruker Faraday balance with 1-μg sensitivity using $HgCo(SCN)_4$ as calibrant.[7] Values of μ_{eff} in Bohr magnetons (μ_B) are reported below with the temperature at which the measurement was made and the diamagnetic correction (χ^{dia})[8] used in the calculation given in parentheses. The cgs emu units

* To whom correspondence should be addressed at the University of Denver.

(1) Eaton, G. R.; Eaton, S. S. *Coord. Chem. Rev.* **1978**, *26*, 207–62.
(2) DuBois, D. L.; Eaton, G. R.; Eaton, S. S. *Inorg. Chem.* **1979**, *18*, 75–9 and references therein.
(3) DuBois, D. L.; Eaton, G. R.; Eaton, S. S. *J. Am. Chem. Soc.* **1979**, *101*, 2624–7.
(4) More, K. M.; Eaton, G. R.; Eaton, S. S. *Inorg. Chem.* **1979**, *18*, 2492–6.
(5) Boymel, P. M.; Eaton, G. R.; Eaton, S. S. *Inorg. Chem.* preceding paper in this issue.
(6) The following abbreviations are used throughout the text: Cu(hfac)$_2$, bis(hexafluoroacetylacetonato)copper(II); NO, a nitroxyl group; py, pyridine; py⁓NO, a ligand which contains both a pyridine and a nitroxyl group; Cu(hfac)$_2$(NO), Cu(hfac)$_2$ bonded to a nitroxyl oxygen; Cu(hfac)$_2$(py⁓NO), Cu(hfac)$_2$ bonded to the pyridine end of py⁓NO; Cu(hfac)$_2$(NO⁓py), Cu(hfac)$_2$ bonded to the nitroxyl group of py⁓NO; Cu(hfac)$_2$(py⁓NO)Cu(hfac)$_2$, a dimer with one Cu(hfac)$_2$ bonded to the pyridine end and one Cu(hfac)$_2$ bonded to the nitroxyl end of py⁓NO; ϵ, molar extinction coefficient at 775 nm; ϵ_{Cu}, ϵ for Cu(hfac)$_2$; ϵ_{py}, ϵ for Cu(hfac)$_2$py or Cu(hfac)$_2$(py⁓NO); $\epsilon_{(py)_2}$, ϵ for Cu(hfac)$_2$(py)$_2$ or Cu(hfac)$_2$(py⁓NO)$_2$; ϵ_{NO}, ϵ for Cu(hfac)$_2$(NO) or Cu(hfac)$_2$(NO⁓py).
(7) Brown, D. B.; Crawford, V. H.; Hall, J. W.; Hatfield, W. E. *J. Phys. Chem.* **1977**, *81*, 1303–6.
(8) Boudreaux, E. A., Mulay, L. N., Eds. "Theory and Applications of Molecular Paramagnetism"; Wiley: New York, 1976.

0020-1669/80/1319-0735$01.00/0